Coarse-grained density functional theory of order-disorder phase transitions in metallic alloys

Ezio Bruno,* Francesco Mammano, and Beniamino Ginatempo
Dipartimento di Fisica, Università di Messina, Salita Sperone 31, 98166 Messina, Italy
(Received 28 April 2009; published 20 May 2009)

The technological performances of metallic compounds are largely influenced by atomic ordering. At finite temperatures metallic alloys are not perfectly ordered nor ideally disordered. Although there is a general consensus that successful theories of metallic systems should account for the quantum nature of the electronic glue, existing nonperturbative high-temperature treatments are based on effective classical atomic Hamiltonians. We propose a solution for the above paradox and offer a fully quantum mechanical, though approximate, theory that on equal footing deals with both electrons and ions. Thus, the amount of order and the electronic properties of metallic alloys are self-consistently determined as a function of the temperature. Our formulation is based on a coarse-grained version of the density functional theory and a Monte Carlo technique, which are jointly implemented allowing for the efficient evaluation of finite temperature statistical averages. Calculations of the relevant thermodynamic quantities and of the electronic structures for CuZn and Ni_3V support that our theory provides an appropriate description of order-disorder phase transitions.

DOI: 10.1103/PhysRevB.79.184204 PACS number(s): 64.60.Cn, 31.15.E−, 71.23.−k, 71.55.Ak

I. INTRODUCTION

Ground-state properties of metallic alloys are routinely calculated by using density functional theory,[1,2] which appropriately incorporates electronic correlations. However, most finite temperature status-of-the-art calculations[3] are based on classical Ising models that, while allow for the accurate evaluation of phase equilibria, cannot predict electronic properties. A theory able to cope with both tasks must incorporate quantum mechanics and should be able to explore the very large space of alloy configurations[4] in order to give reliable statistical averages. Recent density functional theory algorithms[5–8] made feasible the study of supercells containing hundreds or thousands of atoms; however, their application remains bounded to the specific model of disorder implicitly assumed by the supercell choice. Similar arguments also apply to nonlocal extensions of the coherent potential approximation (CPA) theory.[9,10] In principle, quantum simulations as the Car-Parrinello molecular dynamics (CPMD) (Ref. 11) could be able to *ab initio* determine the amount of disorder as a function of the temperature, but unfortunately, their application to metallic alloys and phase equilibria is very hard. In this paper we shall outline an approach to the problem which, similarly to CPMD, is based on the density functional theory and the Born-Oppenheimer approximation, but where the relevant quantities shall be obtained as statistical averages (by sampling the space of alloy configurations) rather than as Boltzmann time averages. Applications to the order-disorder transitions in CuZn and Ni_3V alloys illustrate the flexibility of our approach and show that it is able to obtain a coherent picture of the temperature dependence for both electronic and atomic degrees of freedom.

Although the generalization to n-ary systems is straightforward, in this paper we focus on binary metallic alloys A_cB_{1-c}. They shall be studied in the (T,c) statistical ensemble defined by the temperature T and the mean atomic concentration c. In order to have a tractable problem, we shall limit ourselves to the solid state and the normal metal regime or, equivalently, to the temperatures between the superconducting and the melting transitions, $T_{SC}<T<T_M$. Furthermore, martensitic and magnetic phenomena shall not be considered. The following of the present paper is organized as follows. In Sec. II the approximations that allow to derive our method from the density functional theory are illustrated and the basic algorithms implementing our calculations are discussed; in Sec. III results for the order-transition in CuZn and Ni_3V alloys are presented. In the final Sec. IV we draw our conclusions.

II. THEORY

A. Coarse-grained density functional and charge excess functional Hamiltonian

Our first crucial step is to obtain a *coarse-grained* version of the Hohenberg-Kohn density functional. If the ions constituting the system are considered frozen on the sites of a simple lattice at their equilibrium positions, $\mathbf{R}_i$, then the electrostatic contribution to the density functional can be written as a sum of *local* terms plus some *bilinear* terms involving the *local moments* of the electronic density:[8,12]

$$U^{\mathrm{el}}\{[\rho(\mathbf{r})]\} = \sum_i u_i\{[\rho_i(\mathbf{r})]\} + \frac{e^2}{2}\sum_{i,j} q_i M_{ij} q_j. \qquad (1)$$

In Eq. (1), each lattice site is associated with a Voronoi polyhedron (VP), i.e., to the set of points closer to that particular rather than to any other lattice site, the $u_i([\rho_i(\mathbf{r})])$ are known functionals of the local electronic density, $\rho_i(\mathbf{r})$ and $-eq_i$ are the charge multipole moments in each VP, and the Madelung matrix, $\mathbf{M}$, is determined by the crystal geometry only. As commented in Ref. 8, the coupling between different VP's in Eq. (1) is *marginal*, in the sense that it has a simple, analytically tractable form. Within the popular local density approximation (LDA), the exchange-correlation energy[13] also consists of sums of local electronic density functionals. However, the local kinetic contributions to the density functional are nontrivially entangled by the boundary conditions (bc) that the wave function, or the Green's function,[14] must

match at the VP surfaces. A marginally coupled density functional then requires an approximation for the kinetic part. The literature reports several ways in which such decoupling has been obtained: Ref. 15 uses vacuum bc's, while random bc's are employed in Ref. 16. In our approach the "true" bc's are replaced by appropriate mean field bc's.[8] The same procedure defines the class of the generalized CPA theories (GCPA), whose prototype, the isomorphous CPA (ICPA), has been introduced many years ago by Soven.[17] The ICPA provides an excellent picture[18] of the spectral properties of metallic alloys but may lead to incorrect predictions about the electrostatics.[19] Modern GCPA schemes such as the polymorphous CPA (PCPA) (Ref. 7) heal the shortcomings of the old ICPA model and provide fairly good total energies both for ordered and disordered alloy configurations.[8] We shall then use the GCPA density functional:[8]

$$\Omega^{\mathrm{GCPA}}([\rho_i(\mathbf{r})],\mu;\{\xi\}) = \sum_i \omega^{\alpha}([\rho_i(\mathbf{r})]) + \frac{e^2}{2}\sum_{ij} q_i \mathbf{M}_{ij} q_j - \mu \sum_i q_i. \tag{2}$$

In Eq. (2), the dependence on the alloy configuration is identified by the set of occupation numbers $\{\xi\}$, with $\xi_i=1$ (or 0) for sites occupied by an A (or B) atom. In the case of a simple lattice, the local functionals $\omega^{\alpha}([\rho_i(\mathbf{r})])$ parametrically depend on the site chemical occupation only, $\alpha=A$ or B. Minimizing Eq. (2) with respect to the $\rho_i(\mathbf{r})$ provides a set of Euler-Lagrange equations coupled only through the Madelung potentials, $V_i=\Sigma_j M_{ij} q_j$, and the chemical potential μ:

$$\frac{\delta\omega^{\alpha}}{\delta\rho_i(\mathbf{r})} + e^2 V_i = \mu. \tag{3}$$

Within the alloy sample specified by $\{\xi\}$, due to Eq. (3) and to the variational properties of the GCPA density functional,[8,20,21] the local charge densities for each chemical component, $\rho^{\alpha}(\mathbf{r})$, are *unique functions*[8] of the Madelung potentials. By virtue of the Hohenberg-Kohn theorem, the same holds for any other local physical observable,

$$\langle O\rangle_i = O^{\alpha}(V_i). \tag{4}$$

Evidently, also the charge moments, q_i, are unique functions of the V_i. If, as it can be argued on a physical ground, the qV laws, $q_i=q^{\alpha}(V_i)$, are strictly monotonic,[8] then they can be inverted, thus allowing to recast the first term in Eq. (2) as a *function* of the charge moments rather than a *functional* of the full charge density, $\omega^{\alpha}([\rho_i(\mathbf{r})]) \rightarrow \tilde{\omega}^{\alpha}(q_i)$. This gives the desired coarse graining.

Actually, in the metallic state, the qV laws are not only monotonic but numerically almost indistinguishable from straight lines.[8,22,23] Thus, an excellent approximation for Eq. (2) can be obtained by a series expansion about the zero-field (or ICPA) values of the charge moments, q_i^0. This gives the

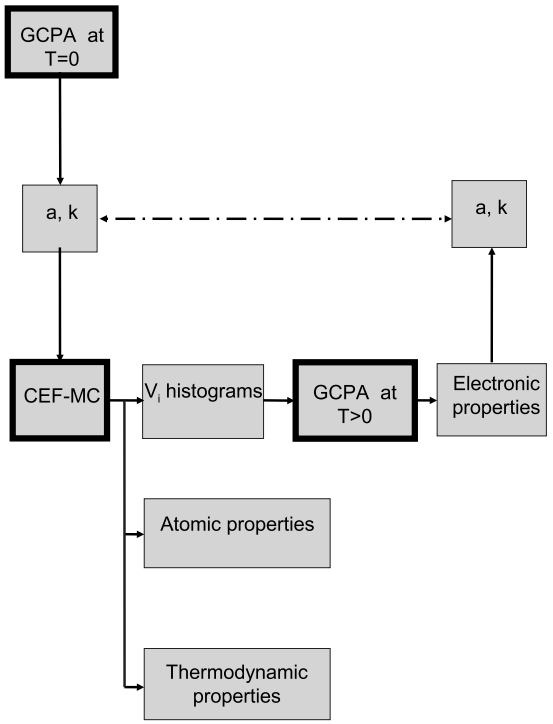

FIG. 1. Flow chart illustrating the GCPA-CEF-MC algorithm. The three main steps of the algorithm are highlighted by thick lines.

charge excess functional (CEF) already obtained on a phenomenological ground in Ref. 23,

$$\Omega^{\mathrm{CEF}}(\{q\},\mu;\{\xi\}) = \sum_i \frac{a_i}{2}(q_i - q_i^0)^2 + \frac{e^2}{2}\sum_{ij} q_i M_{ij} qj - \mu\sum_i q_i, \tag{5}$$

where $a_i=[d^2\tilde{\omega}^{\alpha}(q)/dq^2]_{q=q_0}$ takes the values a_A or a_B, depending on the site occupation. For a given configuration, $\{\xi\}$, the minimum value of the functional in Eq. (2) or Eq. (5) corresponds to the total system energy and, therefore, provides an *ab initio* effective atomic Hamiltonian.[23] Unlike most Ising models, such CEF Hamiltonian[24] includes effective interactions at all distances and n-body interactions up to any value for n. For a binary alloy, it is determined by only three concentration-dependent parameters that can be easily obtained by GCPA density functional calculations as described in Ref. 8.

B. Generalized coherent potential approximation charge excess functional Monte Carlo method

In this paper we implement a coarse-grained all-electrons theory based on the GCPA density functional and a finite temperature Monte Carlo (MC) sampling[25,26] of the alloy configurations space. A flux diagram of the theory, in the following referred to as GCPA-CEF-MC, is shown in Fig. 1. GCPA-CEF-MC calculations consist of three major stages:

(i) The GCPA density functional is determined by $T=0$ electronic structure calculations.

(ii) For a given thermodynamic point (T,c) the relevant ensemble of configurations is sampled by a MC based on the

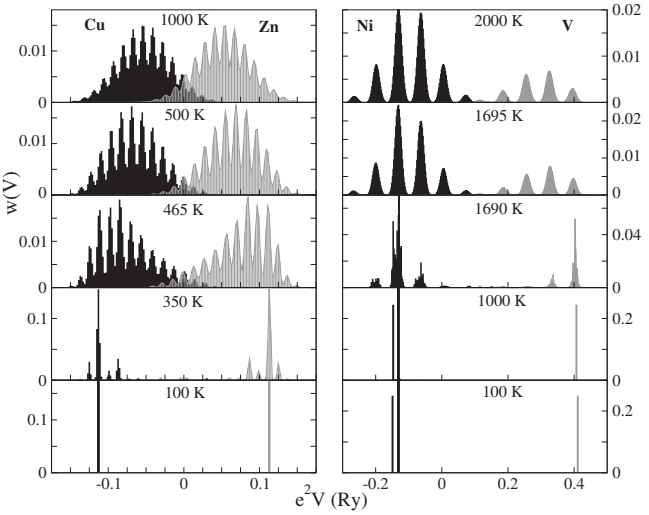

FIG. 2. Distributions of the Madelung potentials (DMP). Calculated DMP's for CuZn (left) and Ni_3V (right) alloys at the indicated temperatures. The structures visible in the DMP's are associated with the local atomic environments. Above the transition temperature ($T_O \approx 465$ K for CuZn and $T_O = 1701 \pm 11$ K for Ni_3V) the DMP's present an overall Gaussian shape, while at lower temperatures they resemble the $T \to 0$ limit, consisting of δ-like peaks, one for each nonequivalent lattice site.

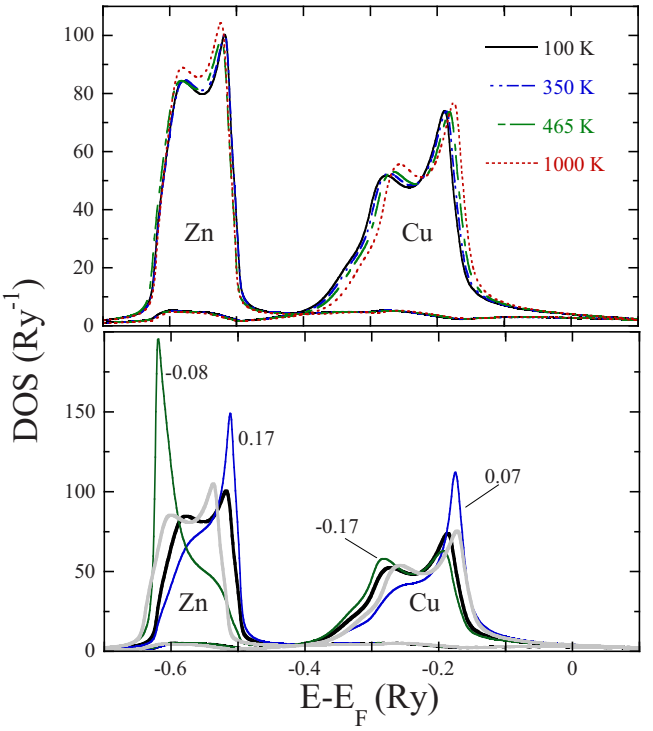

FIG. 3. (Color online) Site resolved electronic DOS's for CuZn alloys. Upper frame: mean DOS contributions from Cu and Zn sites at the indicated temperatures. Lower frame: the comparison between the mean DOS's from Cu and Zn sites at $T = 350$ K (thick black lines) with those from the most extreme chemical environments in the GCPA ensemble (light lines, the corresponding values for e^2V_i are indicated by the labels) shows the sensitivity of the theory to the site environments. The lower frame reports also the ICPA site resolved DOS evaluated at the same lattice constant (thick gray lines).

CEF Hamiltonian; for each configuration, the local charges and Madelung potentials are obtained by minimizing Eq. (5) whose solutions are numerically indistinguishable[8] from those of Eq. (2). The same stage provides the ensemble averages corresponding to the relevant thermodynamic quantities and to the properties related with the atomic degrees of freedom only, such as, e.g., the pair-correlation functions.

(iii) The distribution of the Madelung potentials (DMP) obtained at stage (II) (see Fig. 2) then allows for the evaluation of the appropriate ensemble averages for the electronic properties through Eq. (4).

The details of the practical implementation of the above three steps are presented in Appendix A. We wish to highlight here a point of conceptual importance. A GCPA theory requires a model,[8] i.e., the weights to be assigned to different atomic environments. The DMP, obtained at the stage (ii) above, actually provides the statistical weights to be given to each atomic environment, thus, at variance of existing GCPA theories, the present theory avoids any arbitrary model and the electronic properties obtained at the stage (iii), such as the DOS's shown in Fig. 3, are then free of any *a priori* assumption about the ordering status of the alloy under consideration.

III. RESULTS FOR CuZn AND Ni_3V ALLOYS

In order to test our GCPA-CEF-MC method, we have selected two well studied systems: CuZn,[10,27,28] already discussed by Landau[29] as the prototype for his theory of second-order phase transitions and Ni_3V,[30,31] for which there is competition between different ordered structures. For both alloys thermal expansion has been included.[32] However, this inclusion implies only small quantitative changes to our results. The details of our calculations are given in Appendix A.

Below T_M, both systems present disordered solid solution phases based on the relatively open bcc lattice for CuZn and on the close-packed fcc for Ni_3V. On decreasing T, both systems undergo a transition to the ordered phases, B_2 and $D0_{22}$ respectively (see Appendix B). The phase transitions have been monitored by plotting the total energies and the specific heats as a function of T (Fig. 4).

The calculations for CuZn alloys show the neat evidence of an order-disorder transition occurring at $T_O \approx 465$ K, with a smooth dependence on N, the number of atoms contained in the simulation box. The specific heat exhibits the λ shape that is a typical feature of second-order phase transitions, while no hysteresis loop is visible in the trends of the total energies. For this system, detailed data about the temperature dependence of the intensity of the relevant peak of the structure factor, h_{100}, are available from x-ray or neutron-diffraction experiments.[33,34] The comparison with our simulation results, displayed in Fig. 5, shows a very good agreement. In particular, the comparison is excellent above T_O, while, below T_O, it is more difficult since the strong T dependence of x-rays Cu atomic factors[33] causes a decrease in the experimentally measured h_{100} as $T \to 0$.

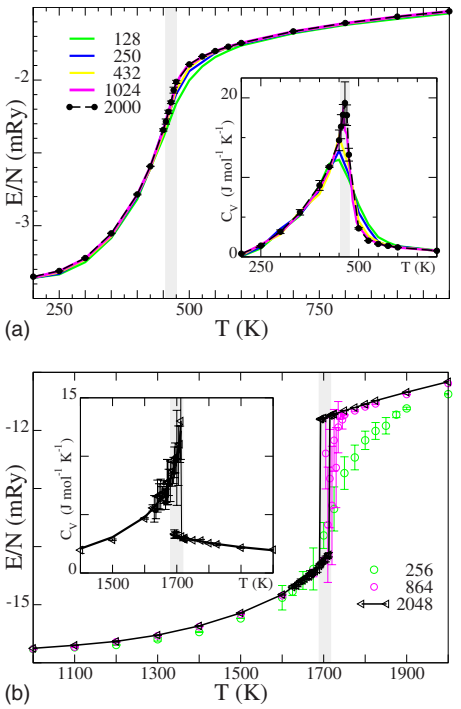

FIG. 4. (Color online) Electronic contributions to the total energies E and the specific heats c_V for CuZn (upper frame) and Ni_3V (lower frame) alloys as a function of the temperature. The specific heats (insets) identify the ordering temperatures, T_O, with the respective uncertainties indicated by the shaded regions. Different symbols refer to different sizes (N) of the simulation boxes.

In the vicinity of the transition, quite large N values are necessary to obtain well converged thermodynamic properties for the Ni_3V system. For the largest simulation box, ordering occurs on cooling between 1692.5 and 1690 K, while, on heating, the low-T state disorders between 1710 and 1712.5 K. Our best estimate for T_O in Ni_3V is then 1701 ± 11 K. This hysteresis loop reveals the first-order character of the symmetry breaking fcc-$D0_{22}$ transition.[35] This is also confirmed by the abrupt change in the structure factor displayed in Fig. 6. These sharp first-order features are gradually suppressed by finite-size effects in the smaller simulation boxes investigated.

Our results demonstrate that the GCPA-CEF-MC theory is able to provide a sensible description of ordering phenomena

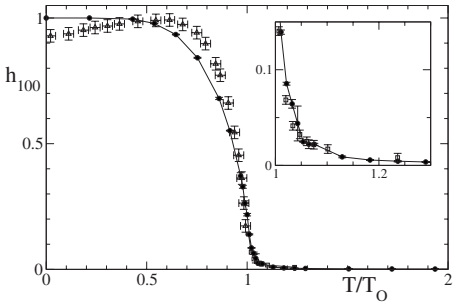

FIG. 5. Temperature dependence of the intensity of the (100) peak of the structure factor, h_{100}, for CuZn alloys. Filled circles: present calculations, open triangles: x-ray measurements (Ref. 33), open squares: neutron-diffraction experiments (Ref. 34).

in metallic alloys. Remarkably, we find complete agreement with the experiment about the low-T ordered phases and the theory correctly discriminates between first- and second-order transitions. The agreement with the experiments about the atomic pair correlation is quantitatively excellent, at least for the CuZn system for which experimental results are available. However, the ordering temperatures obtained from our simulations are not completely satisfactory. The experimental ordering temperatures[36] for CuZn and Ni_3V, 740 K and 1313 K, respectively, are in one case lower and in the other higher than the calculated values. This is probably due to the single-site nature of the GCPA and to the approximations (see Appendix A) made for the site potentials.

IV. CONCLUSIONS

We have presented a theoretical scheme that allows for the simulation of metallic alloys including both electronic and nuclear degrees of freedom. The theory is based on the Born-Oppenheimer approximation and the coarse-grained electronic density functional that we have obtained by applying mean field, GCPA, boundary conditions at the surfaces of conveniently chosen atomic-sized elementary cells.

The results for two different systems, CuZn and Ni_3V, presented in the previous section are very encouraging: the theory appears able to discriminate between first- and second-order phase transitions as well as to reproduce the experimental data on atomic ordering and to evaluate the temperature dependence of the electronic structure. However, the obtained estimates of the transition temperatures are less satisfactory, with relative errors about 30% and 15% for CuZn and Ni_3V, respectively. Possible sources could be the single-site approximation that is implied by the GCPA coarse graining, or the further approximations made in the reported calculations: the atomic sphere approximation for the site potentials (ASA) and the LDA for the exchange-correlation functional. We remark that neither the ASA nor the LDA are necessary to the implementation of our scheme. At similarity of the GCPA,[8] also the present theory is able to deal with space-filling potentials, at the price of including dipole or quadrupole terms in Eq. (5), and non-LDA approximations for the exchange-correlation potential could be used, provided they are local in the electronic density or in its gradients.

In summary, we believe that the methodologies presented in this paper offer a route to alloy thermodynamics that fully includes electrons and appreciably enlarges the scales at which quantum mechanics can be applied. The calculations here discussed consider up to 2000 atoms and up to 10^{11} local chemical environments for each point in the (T,c) space. It is clear that such impressive figures can be obtained only because we have a fixed crystal lattice. Our method appears complementary to the CPMD, since it is particularly suitable for the study of diffusive transitions in the solid state. We are confident that, in the next future, coarse-grained density functional theories shall be extended to magnetic metals and to the mesoscopic domain, in order to study defects and plasticity.

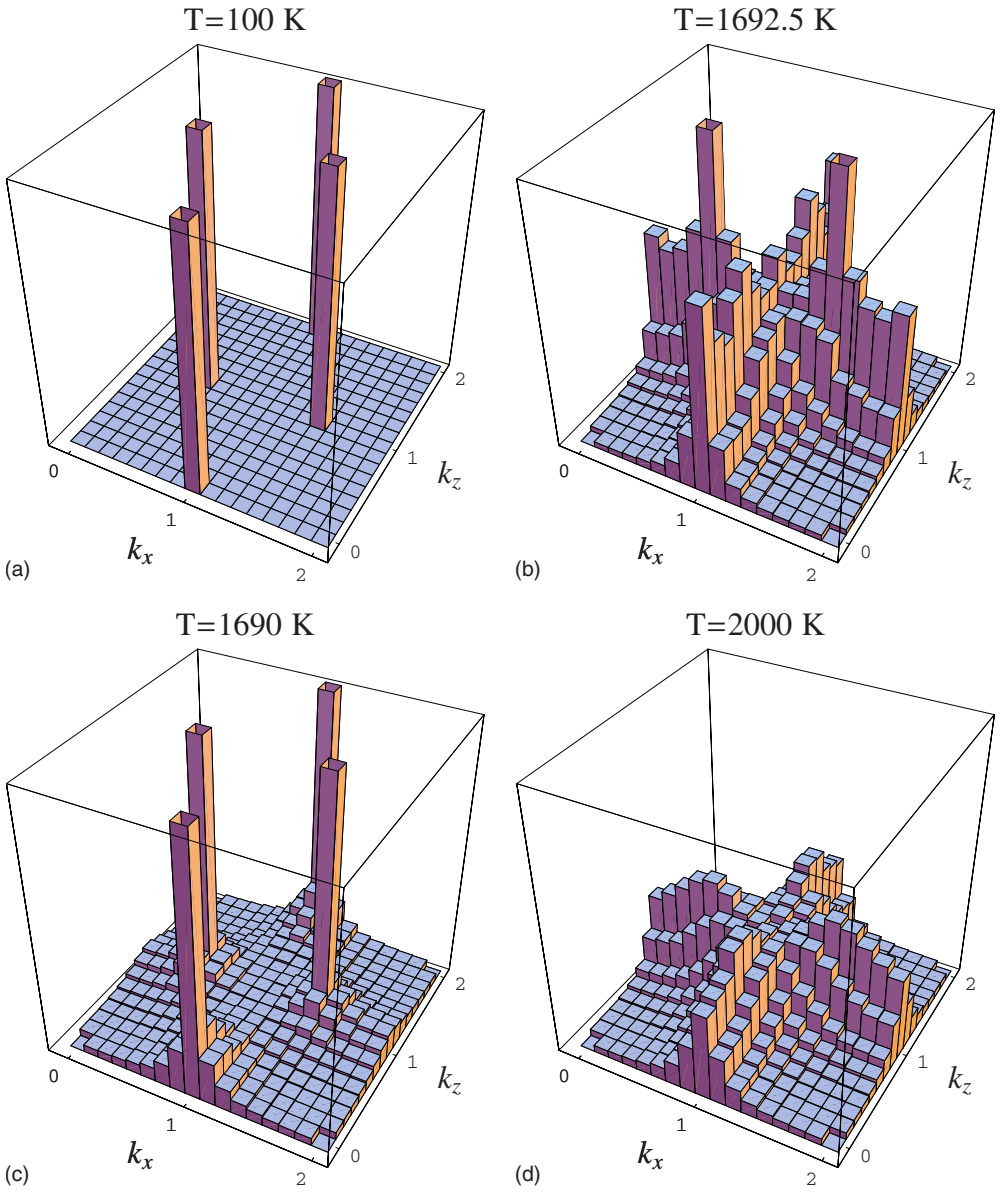

FIG. 6. (Color online) Ni-V partial structure factor for Ni_3V alloys in the $k_y=0$ plane, at the indicated temperatures. Above T_O, the k_x and k_z directions are equivalent, due to the cubic symmetry of the disordered fcc phase. Below T_O, the cubic symmetry is broken, giving rise to the tetragonal symmetry of the $D0_{22}$ structure, with the characteristic peaks at (1,0,0) and (1/2,0,1). It is remarkable the abrupt change in the structure (see Appendix B), that on cooling occurs between 1692.5 and 1690 K.

ACKNOWLEDGMENTS

The calculations presented were executed using the computational facilities located at the CINECA (Bologna, Italy) and at the Consorzio COMETA, project PI2S2 (http://www.pi2s2.it).

APPENDIX A: DETAILS OF CALCULATIONS

1. Determination of the CEF coefficients from GCPA calculations at $T=0$

The starting point are GCPA electronic structure calculations executed at $T=0$. These allow to evaluate the GCPA density functional, Eq. (2), or the CEF functional, Eq. (5), through the CEF coefficients, a_α and k_α, where $\alpha=A,B$ indicate the chemical species. In fact, by minimizing Eq. (5) with respect to the local charge excess, q_i, using also the definition of the Madelung potentials, we obtain

$$a_\alpha(q_i - q_\alpha^0) + e^2 V_i = \mu. \tag{A1}$$

The above equation has the same form as Eq. (1) of Ref. 23 with the identification

$$k_\alpha = a_\alpha q_\alpha^0 + \mu. \tag{A2}$$

The coefficients a_α and k_α can then be obtained by a linear regression of the GCPA output for the site charge moments and Madelung potentials evaluated at the appropriate lattice constants. While the a_α depend only on the mean atomic concentrations and the lattice geometry, the constants

k_α depend also on the specific sample used in the GCPA calculations, through the chemical potential μ. However, as shown in Ref. 23, the k's enter in the CEF expression for the total energy of a binary alloy, A_cB_{1-c}, only through the difference $\Delta k=k_A-k_B$, which is independent on the sample. Thus, the CEF Hamiltonian is completely determined by a_A, a_B, and k_A-k_B. The robustness of the above fitting procedure has been commented in Ref. 8.

2. CEF-MC calculations at $T>0$

Once the CEF Hamiltonian coefficients are determined, a Metropolis' lattice MC is used to sample the space of the alloy configurations. Supercells containing N atoms and periodic boundary conditions are used. Each simulation starts from some conveniently chosen configuration, $\{\xi\}$, the total energy of which, $E_{\{\xi\}}$ is evaluated by the CEF Hamiltonian, as described in Refs. 23 and 24. Such evaluation requires the numerical inversion of an $N\times N$ matrix and then, a computational work proportional to N^3, or $O(N^3)$. A MC move consists of an attempt to exchange the chemical occupations of two randomly selected sites, say i and j. Thus, if the two configurations considered are

$$\{\xi\}=\xi_1,\ldots,\xi_i,\ldots,\xi_j,\ldots,\xi_N \tag{A3}$$

and

$$\{\xi'\}=\xi_1,\ldots,\xi_j,\ldots,\xi_i,\ldots,\xi_N \tag{A4}$$

the energy difference $\Delta E=E_{\{\xi'\}}-E_{\{\xi\}}$ is evaluated. Accordingly with Metropolis' rule, the move is accepted with probability $p=\min\{1,\exp(-\frac{\Delta E}{k_BT})\}$. Further details of our MC algorithm shall be discussed in a future publication. Here we just quote its computational performances: only accepted moves require an appreciable amount CPU time scaling as $O(N^2)$. Although these performances are comparable with those of classical simulations with long ranged forces, we highlight that the CEF Hamiltonian used here has a fully quantum mechanical nature because it explicitly contains electrons through their local moments, the q_i.

For each temperature, at least 5000 N configurations are discarded, then statistics is accumulated for the quantities of interest for at least 10 000 N configurations, and the corresponding numerical errors are statistically elaborated. In particular the histograms for the DMP (see Fig. 2) play a crucial role in our theory. Accordingly with the above, at least 10 000 N^2 different atomic environments are considered for each thermodynamic point that, for the largest simulation boxes employed, amounts to about 4×10^{10} environments. We remark that the size of the above analysis has no precedents in electronic structure calculations. Standard methods[26] have been used for the calculation of the mean total energies. The specific heats have been evaluated from the energy fluctuations and the pair-correlation functions by a fast Fourier transform algorithm.

3. Evaluation of temperature-dependent electronic properties: GCPA at $T>0$

In the statistical ensemble specified by (T,c), the above described CEF-MC calculations provide the frequencies, w_i, for the occurrence of each chemical environment that, in a GCPA theory, is specified by the value of the Madelung potential V_i. Examples of such frequencies or DMP are the $w(V)$ plotted in Fig. 2. As stressed in the paper, the expectation values of local electronic properties are unique functions of V_i [see Eq. (4)]. On the other hand, a GCPA theory is determined by the choice of the statistical weights in w_i, as discussed in Ref. 8. Such self-consistent GCPA calculations required minor modifications to our well tested KKR-CPA code.[37] In particular, at the end of each Kohn-Sham iteration, each time the site potentials are reconstructed from the charge density, constant terms V_i are added and each site Green's function is weighted by w_i in order to determine the GCPA coherent medium.

In spite of the simplicity of the above procedure, the effects on local electronic quantities can be huge, as it is evident from a look at the DOS's plotted in the lower frame of Fig. 3. As discussed in Ref. 38, due to the metallic screening and the self-consistent iteration procedure, these effects are not trivial and can be quite large.

Rather than using the full set of values of the V_i generated by the algorithm, it is sufficient to employ sufficiently accurate histograms for the DMP. We have executed test of the convergence of the above procedure with respect to size of the step used in building the histograms, ΔV. We have found that the DOS obtained for $e^2\Delta V=2\times10^{-2}$ Ry and $e^2\Delta V=2\times10^{-3}$ a.u. are almost undistinguishable. This implies that the complex DMP features in Fig. 2 are already reproduced using about ten histograms for each chemical species. For all electronic structure calculations reported in this paper $e^2\Delta V$ has been set to 2×10^{-3} Ry, that implies one or two hundreds histograms for each chemical species.

4. GCPA calculations

All GCPA calculations, see (i) and (iii), have been performed by conveniently modified versions of our KKR-CPA code[37] using the atomic sphere approximation (ASA) for the site potentials, with the atomic spheres volumes fixed to the mean atomic volume. Depending on the amount of structure in the k space, up to 2×10^4 k points in the full Brillouin zone have been used for each of 31 energies over a complex integration contour. The core electrons treatment has been fully relativistic while a scalar relativistic approximation has been used for valence states. The exchange-correlation potential has been approximated by the LDA.

5. Thermal expansion

In this paper, the effects of ionic motion have been included using the Debye-Grüneisen model of Moruzzi *et al.*,[32] one of the simplest treatments able to provide a realistic picture of lattice vibrations and thermal expansion in metals. The relevant quantities in the model are the Debye temperature Θ_D and the Grüneisen constant γ, which can be easily evaluated from the dependence of the calculated total energies on the crystal volume. The obtained values are reported in Table I. As implied by the Born-Oppenheimer approximation which is implicit in the model, the total energy is simply written as the sum of an electronic and a vibrational term.

TABLE I. Calculated and experimental bulk modulus, B, Debye temperature, Θ_D, Gruneisen constants, γ, lattice parameters at 293 K, a_{lat}, and isothermal linear expansion coefficient at 298 K, α_T.

	CuZn		Ni_3V	
Property	Theory	Experiment	Theory	Experiment
B (GPa)	166	145 ± 22 (Ref. 39)	250	124 (Ref. 40)
Θ_D(K)	343	302 ± 1 (Ref. 39)	442	
γ	2.53		1.81	1.15–4.9 (Ref. 40)
a_{lat}(a.u.)	5.426	5.576 (Ref. 41)	6.601	6.693 (Ref. 41)
$\alpha_T(K^{-1})$	9.52	19.1×10^{-6} (Ref. 39)	5.6×10^{-6}	10.6 (Ref. 40)

For each temperature, we used the lattice parameters obtained by the Debye-Grüneisen model and their temperature dependence has been fitted by a Padé approximant. The parameters of the CEF Hamiltonian, a_A, a_B, and $k_A - k_B$, have been obtained as described above from PCPA calculations executed for randomly occupied supercells containing 64 Cu and 64 Zn (81 Ni and 27 V) atoms for CuZn (Ni_3V) alloys. The dependence of the CEF parameters on the lattice constants has been fitted by second-order polynomials. For all CEF calculations the charge multipolar expansion of Ref. 8 has been truncated at $\ell = 0$.

APPENDIX B: THE CRYSTAL STRUCTURES DISCUSSED

In this section we provide some additional information about the crystal structures which are relevant for the order-disorder transitions in CuZn and Ni_3V alloys.

1. CuZn

About the equiatomic concentration CuZn alloys form the so-called β-brass structure, a substitutional solid solution based on the bcc lattice. On decreasing the temperature, at $T_O = 727$ K, the system orders in the β' structure based on the cubic B_2 lattice.[36] According to Khachaturyan[42] this ordering transition can be discussed in terms of the concentration waves generated by the star corresponding to the Lifshitz point $P = \frac{2\pi}{a_{\text{lat}}}(111)$, where a_{lat} is the lattice parameter. Both structures have cubic symmetry. The spatial groups of the ordered and the disordered structures (see Fig. 7) are denoted as $Pm\bar{3}m$ and $Im\bar{3}m$, respectively; the corresponding Pearson symbols are $cP2$ and $cI2$.

2. Ni_3V

At low V concentrations, NiV alloys present a high-temperature phase based on the Ni fcc lattice (space group: $Fm\bar{3}m$, Pearson symbol: $cF4$) with substitutional disorder. On cooling at the stoichiometric composition, Ni_3V, at $T_O = 1318$ K the alloy forms the ordered $D0_{22}$ phase (space group: $I4/mmm$, Pearson symbol: $tI8$). As shown in Fig. 8,

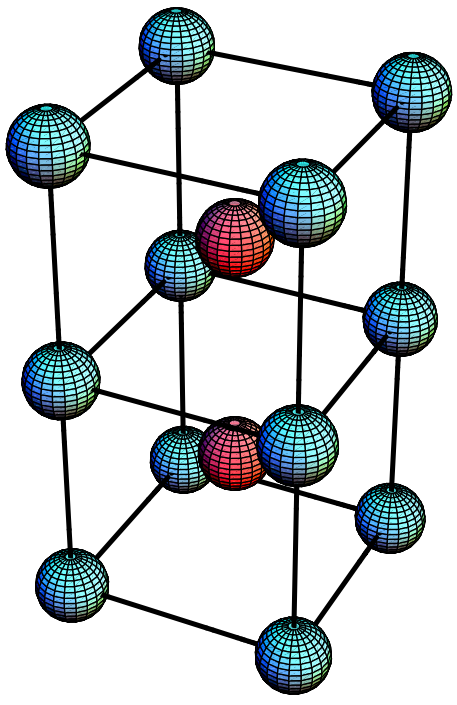

FIG. 7. (Color online) Low-temperature B2 phase for CuZn alloys. Different shading identifies different chemical elements.

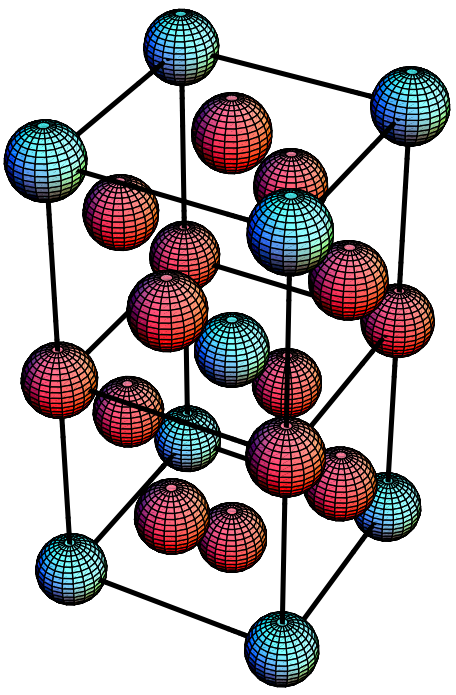

FIG. 8. (Color online) Low-temperature $D0_{22}$ phase for Ni_3V alloys. Different shading identifies different chemical elements.The ordered $D0_{22}$ phase has a tetragonal symmetry.

the ordered phase has a tetragonal symmetry, with the z axis corresponding to the vertical axis in the figure. The crystallographic unit cell is formed by a V atom at $(0,0,0)$, a Ni_1 atom at $(0,0,c_{lat}/2)$, and two crystallographically equivalent Ni_2 atoms at the positions $(a_{lat}/2,0,c_{lat}/4)$ and $(0,a_{lat}/2,c_{lat}/4)$. This is the reason why at the lowest temperatures reported in Fig. 3, two differently charge states for Ni atoms can be recognized. For $c_{lat}/a_{lat}=2$, as assumed in our calculations, the atoms are on the positions of the fcc lattice, this notwithstanding the system has still a tetragonal symmetry. Actually the Ni_3V system is close to this ideal ratio, Pearson's handbook[41] reports $c_{lat}/a_{lat}=2.0362$. The relevant stars generating the fcc-$D0_{22}$ ordering transition is composed by the Lifshitz points $X=\frac{2\pi}{a_{lat}}(100)$ and $W=\frac{2\pi}{a_{lat}}(10\frac{1}{2})$. Due to the reduction in the symmetry when undergoing the transition, three martensitic variants of the $D0_{22}$ phase can form, in correspondence to the three possible orientations of the ordered phase with respect to the parent phase crystal axes. Moreover, the doubling of the unit cell size along the ordered phase z axis makes the new phase formation incompatible with supercells with edge $l_\alpha(\alpha=x,y,z)$ for which all the ratios l_α/a_{lat} are odd numbers. This, and the fact that the above-mentioned three martensitic variants have the same formation energy, makes particularly difficult the MC simulation of the Ni_3V order-disorder transition.

*ebruno@unime.it

[1] P. Hohenberg and W. Kohn, Phys. Rev. **136**, B864 (1964).
[2] W. Kohn and L. J. Sham, Phys. Rev. **140**, A1133 (1965).
[3] P. E. A. Turchi *et al.*, Calphad **31**, 4 (2007).
[4] A. Franceschetti and A. Zunger, Nature (London) **402**, 60 (1999).
[5] Y. Wang, G. M. Stocks, W. A. Shelton, D. M. C. Nicholson, Z. Szotek, and W. M. Temmerman, Phys. Rev. Lett. **75**, 2867 (1995).
[6] I. A. Abrikosov, A. M. N. Niklasson, S. I. Simak, B. Johansson, A. V. Ruban, and H. L. Skriver, Phys. Rev. Lett. **76**, 4203 (1996).
[7] B. Ujfalussy, J. S. Faulkner, N. Y. Moghadam, G. M. Stocks, and Y. Wang, Phys. Rev. B **61**, 12005 (2000).
[8] E. Bruno, F. Mammano, A. Fiorino, and E. V. Morabito, Phys. Rev. B **77**, 155108 (2008).
[9] D. A. Rowlands, J. B. Staunton, B. L. Gyorffy, E. Bruno, and B. Ginatempo, Phys. Rev. B **72**, 045101 (2005).
[10] K. Tarafder, A. Chakrabarti, K. K. Saha, and A. Mookerjee, Phys. Rev. B **74**, 144204 (2006).
[11] R. Car and M. Parrinello, Phys. Rev. Lett. **55**, 2471 (1985).
[12] In Eq. (1) and throughout the present paper, the summations over the angular momentum components are truncated at $\ell=0$ for sake of simplicity.
[13] R. M. Dreizler and E. K. U. Gross, *Density Functional Theory* (Springer-Verlag, Berlin, 1990).
[14] A. Gonis, *Green Functions for Ordered and Disordered Systems* (North-Holland, Amsterdam, 1992).
[15] J. Harris, Phys. Rev. B **31**, 1770 (1985).
[16] F. R. Krajewski and M. Parrinello, Phys. Rev. B **71**, 233105 (2005).
[17] P. Soven, Phys. Rev. **156**, 809 (1967).
[18] I. A. Abrikosov and B. Johansson, Phys. Rev. B **57**, 14164 (1998).
[19] R. Magri, S. H. Wei, and A. Zunger, Phys. Rev. B **42**, 11388 (1990).
[20] D. D. Johnson, D. M. Nicholson, F. J. Pinski, B. L. Gyorffy, and G. M. Stocks, Phys. Rev. Lett. **56**, 2088 (1986).
[21] D. D. Johnson, D. M. Nicholson, F. J. Pinski, B. L. Gyorffy, and G. M. Stocks, Phys. Rev. B **41**, 9701 (1990).
[22] J. S. Faulkner, Y. Wang, and G. M. Stocks, Phys. Rev. B **52**, 17106 (1995).
[23] E. Bruno, L. Zingales, and Y. Wang, Phys. Rev. Lett. **91**, 166401 (2003).
[24] E. Bruno, Mater. Sci. Eng., A **462**, 456 (2007).
[25] M. Metropolis, A. W. Rosenbluth, M. N. Rosenbluth, A. N. Teller, and E. Teller, J. Chem. Phys. **21**, 1087 (1953).
[26] D. P. Landau and K. Binder, *A Guide to Monte Carlo Simulations in Statistical Physics* (Cambridge University Press, Cambridge, England, 2000).
[27] S. Muller and A. Zunger, Phys. Rev. B **63**, 094204 (2001).
[28] P. R. Tulip, J. B. Staunton, D. A. Rowlands, B. L. Gyorffy, E. Bruno, and B. Ginatempo, Phys. Rev. B **73**, 205109 (2006).
[29] L. D. Landau and E. M. Lifshitz, *Statistical Physics, Part I*, 3rd ed. (Pergamon Press, Oxford, 1980).
[30] D. D. Johnson, A. V. Smirnov, J. B. Staunton, F. J. Pinski, and W. A. Shelton, Phys. Rev. B **62**, R11917 (2000).
[31] N. A. Zarkevich and D. D. Johnson, Phys. Rev. Lett. **92**, 255702 (2004).
[32] V. L. Moruzzi, J. F. Janak, and K. Schwarz, Phys. Rev. B **37**, 790 (1988).
[33] D. R. Chipman and C. B. Walker, Phys. Rev. Lett. **26**, 233 (1971).
[34] C. B. Walker and D. T. Keating, Phys. Rev. **130**, 1726 (1963).
[35] D. de Fontaine, Solid State Phys. **34**, 73 (1979).
[36] *ASM Handbook*, edited by H. Baker (ASM International, Materials Park, OH, 1992), Vol. 3, ISBN 0-87170-381-5.
[37] E. Bruno and B. Ginatempo, Phys. Rev. B **55**, 12946 (1997).
[38] E. Bruno, L. Zingales, and A. Milici, Phys. Rev. B **66**, 245107 (2002).
[39] M. Peter, W. Potzel, M. Steiner, C. Schäfer, H. Karzel, W. Schiessl, G. M. Kalvius, and U. Gonser, Phys. Rev. B **47**, 753 (1993).
[40] L. J. Nagel, B. Fultz, J. L. Robertson, and S. Spooner, Phys. Rev. B **55**, 2903 (1997).
[41] P. Villars and L. Calvert, *Pearson's Handbook of Crystallographic Data for Intermetallic Phases* (American Society for Metals, Materials Park, OH, 1985), Vol. I, II, and III.
[42] A. G. Khachaturyan, *Theory of Structural Transformations in Solids* (Wiley, New York, 1983).